Eur. Phys. J. D **31**, 213–219 (2004)
DOI: 10.1140/epjd/e2004-00157-4

THE EUROPEAN PHYSICAL JOURNAL D

Formation of ultracold polar molecules via Raman excitation

E. Taylor-Juarros[1,a], R. Côté[1], and K. Kirby[2]

[1] Physics Department, University of Connecticut, 2152 Hillside Rd., Storrs, CT 06269-3046, USA
[2] ITAMP, Harvard-Smithsonian Center for Astrophysics, 60 Garden Street, Cambridge, MA 02138, USA

Received 31 August 2004
Published online 23 November 2004 –

Abstract. Alkali hydride molecules are very polar, exhibiting large ground-state dipole moments. As ultracold sources of alkali atoms, as well as hydrogen, have been created in the laboratory, we explore theoretically the feasibility of forming such molecules from a mixture of the ultracold atomic gases, employing a two-photon stimulated radiative association process — Raman excitation. Using accurate molecular potential energy curves and dipole transition moments, we have calculated the rate coefficients for populating all the vibrational levels of the $X^1\Sigma^+$ state of LiH via the excited $A^1\Sigma^+$ state. We have found that significant molecule formation rates can be realized with laser intensities and atomic densities that are attainable experimentally. Because of the large X state dipole moment, rapid cascade occurs down the ladder of vibrational levels to $v = 0$. The calculated recoil momentum imparted to the molecule is small, and thus negligible trap loss results from the cascade process. This allows for the build-up of a large population of $v = 0$ trapped molecules.

PACS. 34.50.Rk Laser-modified scattering and reactions – 32.80.Pj Optical cooling of atoms; trapping – 33.20.Vq Vibration-rotation analysis

1 Introduction

Over the last several years, formation of ultracold alkali dimers such as Li_2, Na_2, K_2, Rb_2 and Cs_2 has been explored both experimentally and theoretically. Recently, Bose-Einstein Condensates of molecules have been observed [1–4]. There is considerable interest, however, in the creation of ultracold polar molecules, because of novel effects [5] due to dipole-dipole interactions which are predicted to occur. The focus of a number of recent studies has been the creation of mixed alkali species, such as: KRb [6–9], RbCs [10–12], or LiCs [13], from mixtures of the ultracold atomic gases. Alkali hydride molecules, however, have dipole moments which are significantly larger than those of the mixed alkali diatomics.

We have previously explored the formation of ultracold LiH and NaH by one-photon stimulated radiative association, involving transitions directly from the vibrational continuum to specific vibration-rotation levels in the ground state [14]. This process is not possible in the formation of homonuclear diatomic molecules because such systems lack a dipole moment. Experimental efforts are also underway to produce cold LiH using laser ablation and buffer gas cooling [15].

In this work we study the formation of lithium hydride molecules, using a two-photon stimulated Raman photoassociation scheme, starting from mixtures of the ultracold atomic gases, Li and H, which have been separately cooled to ∼1 mK. Because of large dipole transition moments, LiH can serve as a favorable benchmark system with which to explore the feasibility of forming ultracold polar molecules using a two-photon photoassociation scheme. Here, we limit ourselves to the formation of singlet ground state LiH molecules only. Such molecules might be produced in a magneto-optical trap (MOT) or in an all-optical trap. In a purely magnetic trap, the spin-aligned atoms would necessitate consideration of the triplet manifold of states.

2 Process

We will explore the rate of molecule formation through excitation of the colliding Li and H atoms in the ground state $X^1\Sigma^+$ channel to bound vibrational levels of the $A^1\Sigma^+$ state and stimulated emission to bound vibrational levels in the $X^1\Sigma^+$ state. The process is illustrated schematically in Figure 1. Two atoms with energy ε approach each other along the ground electronic state $X^1\Sigma^+$, while two photons with frequencies ν_1 and ν_2 stimulate a transition into a bound rotation-vibration level v of the ground state $X^1\Sigma^+$. Because only s-wave scattering occurs at ultracold temperatures, only $(v', J' = 1)$ ro-vibrational states of the intermediate state $A^1\Sigma^+$ are relevant, and final $(v, J = 0)$ or $(v, J = 2)$ ro-vibrational states of $X^1\Sigma^+$

[a] e-mail: eliztj@phys.uconn.edu

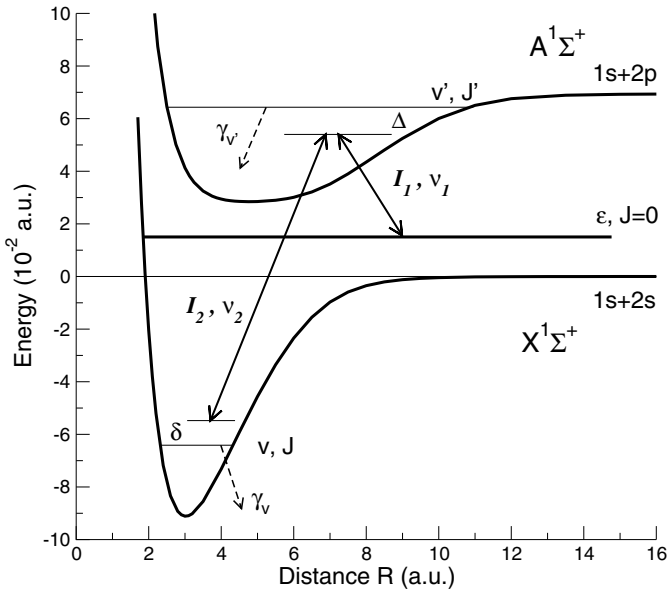

Fig. 1. Schematics of two-photon stimulated Raman molecule formation. The relevant transitions between the two electronic states of LiH are indicated by the double arrows, and the laser frequencies and intensities for the two photons are shown as ν_1, ν_2, and I_1 and I_2.

can be populated. We will focus our attention on the formation rate for $(v, J = 0)$; the rates for $(v, J = 2)$ are of comparable magnitude.

3 Theory

We consider the stimulated Raman photoassociation process shown in Figure 1, where two colliding atoms in a continuum state with energy ε are stimulated to a final molecular bound level v by a pair of lasers L_1 and L_2 with intensities I_1 and I_2, and frequencies ν_1 and ν_2, respectively. Here, Δ and δ correspond to the detunings of L_1 and L_2, associated with the transitions $\varepsilon \to v'$, and $\varepsilon \to v$, respectively.

In this work, we are interested in producing ultracold ground state singlet molecules in a target ro-vibrational state $|v, J = 0\rangle$ of $X^1\Sigma^+$ starting from a continuum state $|\varepsilon, J = 0\rangle$ of $X^1\Sigma^+$, via an intermediate ro-vibrational state $|v', J' = 1\rangle$ of the excited electronic state $A^1\Sigma^+$. If the value of Δ is large compared to the natural width $\gamma_{v'}$ of the intermediate level v', one can write, using an effective Rabi frequency, the two-photon Raman rate coefficient $\mathsf{K}^{(2)}$ in terms of the one-photon photoassociation rate $\mathsf{K}^{(1)}$ to v' and the ratio of the bound-bound Rabi frequency $\Omega_{vv'}$ and the detuning Δ (e.g., see [16])

$$\mathsf{K}^{(2)}_{vv'}(T, \{L\}) = \mathsf{K}^{(1)}_{v'}(T, I_1, \delta) \left(\frac{\Omega_{vv'}}{\Delta}\right)^2 , \qquad (1)$$

where $\{L\} \equiv \{L_1, L_2\}$ implies the various laser parameters. Clearly, this approximate expression fails when $\Delta \to 0$; if $\Delta/\gamma_{v'}$, the ratio of the detuning to the spontaneous decay width of level v', is not large enough, Autler-Townes splittings [17] and large spontaneous decays would need to be taken into account.

The one-photon photoassociation rate $\mathsf{K}^{(1)}$ is obtained following the standard procedure [17,18]

$$\mathsf{K}^{(1)}_{v'}(T, I_1, \delta) = \left\langle \frac{\pi v_{\rm rel}}{\kappa^2} \sum_{J=0}^{\infty} (2J+1) |S_{J,v'}(\varepsilon, I_1, \delta)|^2 \right\rangle , \qquad (2)$$

where $\varepsilon = \hbar^2\kappa^2/2\mu = \mu v_{\rm rel}^2/2$, μ is the reduced mass, $v_{\rm rel}$ is the relative velocity of the colliding pair, and $S_{J,v'}$ represents the scattering matrix element for producing the state v' from the continuum state. At ultracold temperatures, only the s-wave $(J = 0)$ contributes, and the sum over partial waves J contains only one term. Averaging over relative velocities is implied by $\langle \dots \rangle$, and assuming a Maxwellian velocity distribution characterized by the temperature T, $\mathsf{K}^{(1)}_{v'}(T, I_1, \delta)$ at ultralow-T becomes

$$\mathsf{K}^{(1)}_{v'}(T, I_1, \delta) = \frac{1}{hQ_T} \int_0^{\infty} d\varepsilon \; e^{-\varepsilon/k_BT} |S_{J=0,v'}(\varepsilon, I_1, \delta)|^2 , \qquad (3)$$

where $Q_T = \left(2\pi\mu k_B T/h^2\right)^{3/2}$ (k_B is the Boltzmann constant). The scattering matrix is well approximated by [17]

$$|S_{J=0,v'}(\varepsilon, I_1, \delta)|^2 = \frac{\gamma_{v'}\gamma_s(\varepsilon, J=0)}{[(\varepsilon-\delta)^2 + (\gamma/2)^2]} , \qquad (4)$$

where $\gamma = \gamma_{v'} + \gamma_s$. Here $\gamma_{v'}$ is the width of the intermediate bound level $(v', J' = 1)$ and γ_s is the stimulated width from the continuum initial state $|\varepsilon, J = 0\rangle \equiv |\varepsilon\rangle$ to the state $|v', J' = 1\rangle \equiv |v'\rangle$. At low laser intensities, we write

$$\gamma_s(I_1, \varepsilon, v') \simeq 4\pi^2 \frac{I_1}{c} |D_{v'}(\varepsilon)|^2 = 2\pi\hbar^2 \Omega^2_{\varepsilon v'} , \qquad (5)$$

where $|D_{v'}(\varepsilon)|^2 \equiv |\langle v'|D(R)|\varepsilon\rangle|^2$ is the square of the dipole transition matrix element, $D(R)$ is the molecular dipole transition moment connecting the ground and excited electronic states, and $\Omega_{\varepsilon v'}$ is the Rabi frequency between the continuum and bound states. Here, we follow the convention of [17], i.e. the Rabi frequency is defined as $\Omega \equiv E_{\rm max} d/2\hbar$, where $d = \langle f|D(R)|i\rangle$ is the dipole transition matrix element between the initial energy-normalized continuum state wavefunction ($|i\rangle$) and final bound ($|f\rangle$) states and $E_{\rm max}$ is the amplitude of the oscillating electric field. From the definition of the intensity $I = \epsilon_0 c E^2_{\rm max}/2$, where ϵ_0 is the vacuum permittivity, we can write $\hbar\Omega = d\sqrt{I/2\epsilon_0 c} = d\sqrt{2\pi I/c}$ (using $4\pi\epsilon_0 = 1$ in C.G.S units), and hence equation (5). Note that the units of $\hbar\Omega_{\varepsilon v'}$ are Joules$^{1/2}$, due to the energy normalized continuum function appearing in d.

If $\gamma_s/\gamma_{v'} \ll 1$ (which is satisfied in our case — see Sect. 5), we can approximate $|S_{J=0,v'}|^2$ by

$$|S_{J=0,v'}(\varepsilon, I_1, \delta)|^2 \simeq 2\pi\gamma_s(I_1, \varepsilon, v')\delta(\varepsilon - \delta) , \qquad (6)$$

and equation (3) takes the simple form

$$\mathsf{K}^{(1)}_{v'}(T, I_1, \delta) = \frac{2\pi}{hQ_T} e^{-\delta/k_BT} \gamma_s(I_1, \delta, v') . \qquad (7)$$

In the ultralow energy limit, we also find that $|D_{v'}(\varepsilon)|^2 = C_{v'}\sqrt{\varepsilon}$, so that $\gamma_s \propto \sqrt{\varepsilon}$, in accordance with Wigner's threshold law [19]. Therefore, $\mathsf{K}^{(1)} \propto e^{-\delta/k_BT}\sqrt{\delta}$ which is maximum for $\delta = k_BT/2$. Using this value for the detuning δ and equation (5), we have

$$\mathsf{K}^{(1)}_{v'}(T, I_1) = \frac{8\pi^3}{h}\frac{I_1}{c}\frac{e^{-1/2}}{Q_T}C_{v'}\sqrt{k_BT/2}\,. \qquad (8)$$

Note that we have not accounted for the light polarization in the above expression, which could introduce a factor of 3 into the denominator.

It is straightforward to rederive equation (1) using an effective Rabi frequency for the two-photon process (when Δ is far detuned from v'). In fact, the two-photon rate is then obtained using the one-photon rate above with the Rabi frequency $\Omega_{\rm eff} = \Omega_{\varepsilon v'}\Omega_{v'v}/\Delta$. Writing $\hbar^2\Omega^2_{v'v} = (2\pi I_2/c)|D_{v'v}|^2$, equation (1) becomes

$$\mathsf{K}^{(2)}_{vv'}(T, \{L\}) = \frac{64\pi^6}{h^3}\frac{I_1I_2}{c^2}\frac{e^{-1/2}}{Q_T}\sqrt{\frac{k_BT}{2}}C_{v'}\frac{|D_{v'v}|^2}{\Delta^2}. \qquad (9)$$

4 Potentials and dipole moments

Two molecular electronic states, $X^1\Sigma^+$ and $a^3\Sigma^+$, correlate to ground state alkali-hydrogen pairs, Li(^{2}S) and H(^{2}S). The singlet state is the ground state in all alkali hydride systems, with a binding energy of 2.5154 eV for LiH. We have used the $X^1\Sigma^+$ state potential from [20,21] for LiH, incorporating the correct long range form. For the $A^1\Sigma^+$ state potential energy curve, we have used the curve of [22] (see their Tab. 1): however, the value of the potential at $R = 17.5\ a_0$ was corrected from its published value of $-7.891\,443_{16}$ a.u. to $-7.891\,458_{16}$ a.u. [23]. The inner wall and the long-range form of the potential $-C_6/R^6 - C_8/R^8$ (with coefficients $C_6 = 147.9$ a.u. and $C_8 = 20\,700$ a.u.) that we used are given in Table 3 of reference [22]. Both potential curves are shown in Figure 1.

For the $X^1\Sigma^+$ state, the dipole moment function, $D_X(R)$, was taken from the calculations of Docken and Hinze [24]. The calculated points were fitted using a cubic spline and joined smoothly to the form be^{-cR} at large separations: b and c were found to be 1651.7 a.u. and 0.959 a.u., respectively, by using the data at $R = 10.0\ a_0$ and $12.0\ a_0$. For the $A^1\Sigma^+$ state, the dipole moment function, $D_A(R)$, was taken from the calculations of Partridge et al. [25], fitted by a cubic spline and joined smoothly to the form be^{-cR} at large separations Using the data at $R = 20.0\ a_0$ and $22.5\ a_0$, b and c were found to be 11294.6 a.u. and 0.7554 a.u., respectively. Finally, the dipole transition moment $D_{XA}(R)$ between $X^1\Sigma^+$ and $A^1\Sigma^+$ was taken from [25], fitted using a cubic spline, and joined smoothly to a constant value of 2.3493 a.u. for $R > 20\ a_0$. The constructed curves for the various dipole moments of LiH are shown in Figure 2.

5 Results and discussion

We have computed the widths $\gamma_{v'}$ and lifetimes $\tau_{v'} = \hbar/\gamma_{v'}$ of the ro-vibrational levels $(v', J' = 1)$ for the $A^1\Sigma^+$ state and $(v, J = 0)$ for the $X^1\Sigma^+$ state. They are listed in Tables 1 and 2, respectively. For the $A^1\Sigma^+$ state, the levels can decay by spontaneous emission into lower levels v' in the same electronic state, or into continuum or discrete levels of the ground $X^1\Sigma^+$ state. For the $X^1\Sigma^+$ state, only decay into lower ro-vibrational levels of the same

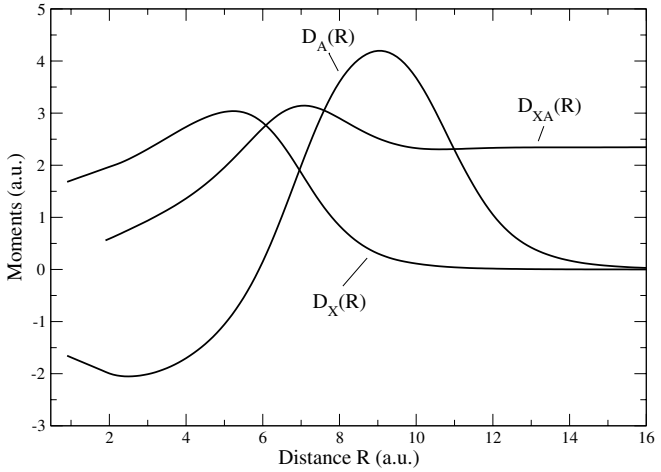

Fig. 2. Dipole moments of the $X^1\Sigma^+$ and $A^1\Sigma^+$ states, and the dipole transition moment between these states.

Table 1. Coefficient $C_{v'}$ of the dipole matrix element $|D_{v'}(\varepsilon)|^2 = C_{v'}\sqrt{\varepsilon}$ for transitions from the continuum of $X^1\Sigma^+$ $(J = 0)$ to bound levels of $A^1\Sigma^+$ $(J' = 1)$ of ^{7}LiH, and lifetimes of the intermediate levels v'. Powers of ten are given in square brackets.

Level	$C_{v'}$	$\tau_{v'}$ (ns)		
v'	(a.u.)	this work	Ref. [25]	Ref. [27]
0	1.853 [–3]	28.78	27.4	28.9
1	3.705 [–1]	29.95	28.4	29.5
2	6.425 [0]	30.78	29.2	30.2
3	1.870 [1]	31.57	29.8	30.8
4	4.445 [1]	32.17	30.4	31.5
5	3.165 [3]	32.84	31.0	32.0
6	1.812 [4]	33.48	31.6	32.6
7	8.639 [3]	34.05	32.1	33.1
8	8.047 [4]	34.57	32.6	33.6
9	6.618 [5]	35.05	33.0	34.2
10	4.984 [5]	35.55	33.3	34.6
11	1.373 [5]	36.03	33.7	35.5
12	1.485 [6]	36.32	34.0	35.7
13	7.678 [5]	36.68	33.8	35.8
14	2.808 [5]	37.00	33.6	35.6
15	7.291 [5]	37.21	32.9	35.4
16	2.269 [5]	37.36	32.3	34.9
17	5.121 [4]	37.35	32.1	34.5
18	3.344 [4]	37.25	31.3	33.7
19	4.581 [5]	37.04	29.9	32.6
20	1.670 [6]	36.59	28.7	31.5
21	1.888 [6]	35.97	27.1	30.4
22	4.616 [6]	35.03	26.2	29.3
23	6.733 [6]	33.76	25.6	28.3
24	1.090 [7]	32.07	24.7	27.5
25	1.935 [7]	29.91	24.0	27.1
26	8.933 [6]	28.10	23.5	27.1

Table 2. Widths and lifetimes for levels (with $J = 0$) in the $X^1\Sigma^+$ state of ^{7}LiH.

Level	τ_v (ms)	
v	this work	Ref. [28]
0	∞	∞
1	22.06	21.77
2	11.71	11.76
3	8.336	8.264
4	6.702	6.623
5	5.757	5.605
6	5.155	4.980
7	4.753	4.559
8	4.472	4.261
9	4.267	4.045
10	4.105	3.886
11	3.959	3.756
12	3.804	3.629
13	3.623	3.478
14	3.417	3.301
15	3.201	3.108
16	3.008	2.932
17	2.879	2.810
18	2.866	2.787
19	3.046	2.935
20	3.557	3.396
21	4.782	4.490
22	8.782	7.984
23	97.96	128.7

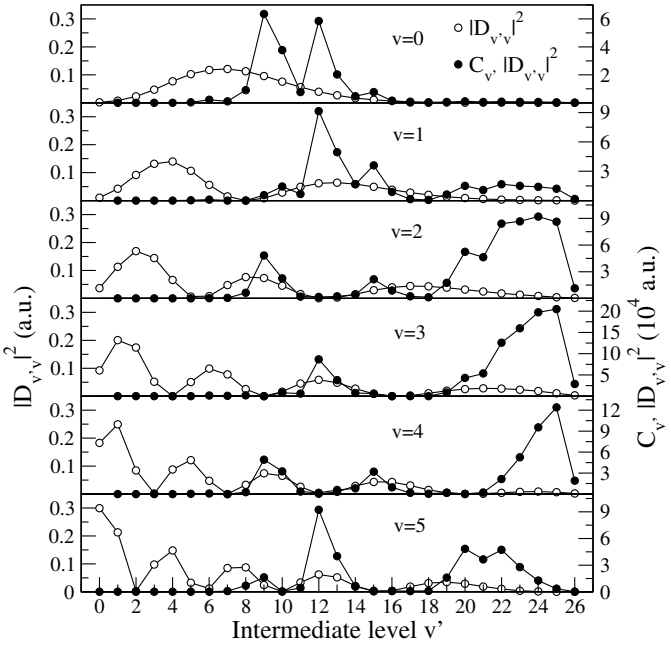

Fig. 3. The squares of the bound-bound dipole transition matrix elements, $|D_{v',v}|^2$, are plotted with open circles, following the left-hand side vertical scale, for values of final X-state $v = 0$ to 5, as a function of the intermediate A state vibrational level v'. The quantities $C_{v'}|D_{v',v}|^2$ are plotted similarly using filled circles and the right-hand side vertical scale.

electronic state is possible. In both cases, we do not take into account quenching to lower levels due to collisions.

For the $A^1\Sigma^+$ state, we found lifetimes of the order of tens of nanoseconds, ranging from 28.8 ns for $v' = 0$ to 37.4 ns for $v' = 16$. The values of $\tau_{v'}$ increase starting at $v' = 0$ and reach a maximum value for $v' = 16$ before decreasing to 28.1 ns for the uppermost level $v' = 26$. This latter value is very close to the Li($2p$) atomic lifetime of 27.102 ns [26], as expected because the $A^1\Sigma^+$ state correlates asymptotically to H($1s$) + Li($2p$). The widths $\gamma_{v'}$ behave as the reciprocal of $\tau_{v'}$. In Table 1 we also list the lifetimes of Partridge and Langhoff (1981) [25] and Zemke, Crooks and Stwalley (1978) [27] and notice that the three sets of values are comparable for $v' = 0{-}9$. Differences arise as v' increases, because of the increasing importance of the continuum levels of the X state in the decay of the higher v' states. We calculated this contribution explicitly, integrating over the full range of continuum energies, whereas both of the other references used an approximate treatment involving a sum over the discrete levels to estimate the decay into the continuum.

For the $X^1\Sigma^+$ state, the values of τ_v, as given in Table 2, initially decrease starting at 22.1 ms for $v = 1$ down to 2.87 ms for $v = 18$, before increasing rapidly to reach 8.78 ms for $v = 22$ and finally 97.97 ms for the last level $v = 23$. This last very large value reflects the poor overlap of the wave function of $v = 23$ with all other levels in regions where the variation of the dipole moment is appreciable. Our calculated values agree well with the published lifetimes of Zemke and Stwalley (1980) [28].

In order to find the largest possible two-photon rate, we need to identify the most favorable combination of X–A free-bound and A–X bound-bound transitions. To that effect, we first computed the X–A free-bound dipole transition matrix elements (squared) to each intermediate level v' of the A-state as a function of the relative collision energy ε, i.e. $|D_{v'}(\varepsilon)|^2$. For $\varepsilon/k_B < 10$ mK, these matrix elements are well approximated by the Wigner [19] threshold form $C_{v'}\sqrt{\varepsilon}$. The values of $C_{v'}$ are listed in Table 1, and were determined by a fit. They depend on the bound-continuum dipole transition matrix element which grows from small values at low v' (where the ground state continuum and excited bound state wave functions overlap poorly) to larger values as the overlap becomes better.

In order for equation (6) to be valid, it is necessary that $\gamma_s/\gamma_{v'} \ll 1$. Using lifetimes of the $A^1\Sigma^+$ state as listed in Table 1, we have verified that for the largest $C_{v'}$ (10^7) and $T \sim 1$ mK, this relationship is satisfied for $I \sim 1$ kW/cm^2. Furthermore, to approximate S by a delta function, it is necessary that $\varepsilon/\gamma_{v'} \gg 1$, again satisfied for $T \sim 1$ mK or more.

We also computed all dipole transition matrix elements for the bound-bound transitions. For each target level v (from 0 to 23), $|D_{v'v}|^2$ is plotted as a function of the intermediate level v' (from 0 to 26) in Figures 3–6. As can be seen on these plots, as v increases from 0 to 4, $|D_{v'v}|^2$ roughly mirrors the nodal structure of the associated wave functions; only one maximum for $v = 0$ located at $v' = 7$ (where the Franck-Condon factor is maximal), then two peaks for $v = 1$ with the largest value at $v' = 4$, then

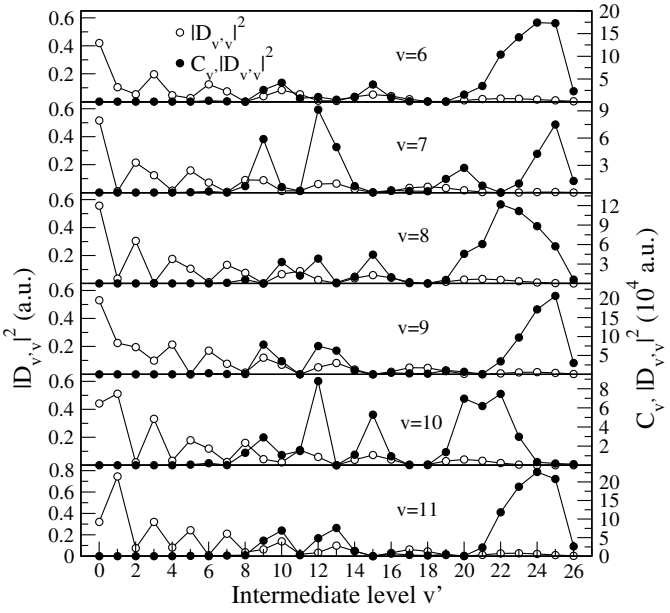

Fig. 4. Same as Figure 3 for $v = 6$ to 11 of the X state.

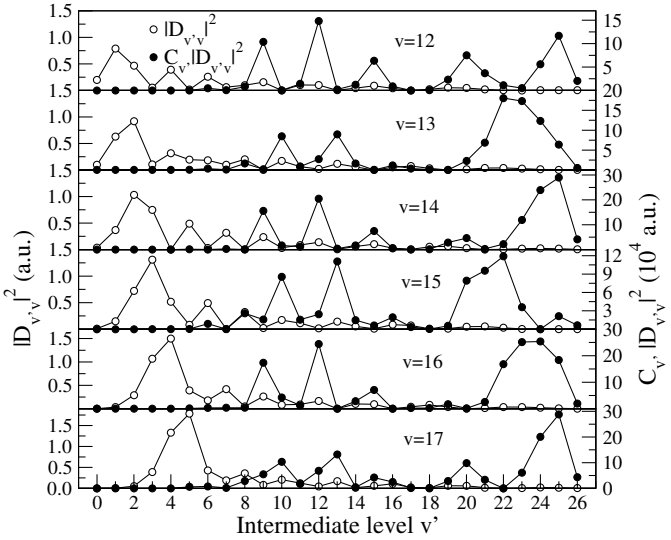

Fig. 5. Same as Figure 3 for $v = 12$ to 17 of the X state.

three peaks for $v = 2$ with the largest value at $v' = 2$, and so on. The value of the largest peak increases slowly from 0.12 a.u. for $v = 0$ to 0.25 a.u. for $v = 4$. For larger v's, the nodal structure is still apparent in $|D_{v'v}|^2$, although the more rapidly oscillatory nature of the wave function prevents the previous simple mapping; the number of oscillations in $|D_{v'v}|^2$ saturates roughly between 5 and 8.

By taking the results for the free-bound and the bound-bound dipole transition matrix elements, we can select the best combinations of states to achieve a particular target level v in the $X^1\Sigma^+$ ground state. From equation (9), the largest two-photon rate coefficient $\mathsf{K}^{(2)}$, for given experimental parameters (I_1, I_2, T, Δ), is obtained when $C'_v|D_{v'v}|^2$ is maximal. In Figures 3–6, we plot this product as a function of the intermediate level v' for a given target state v: the level v' for which the maximal

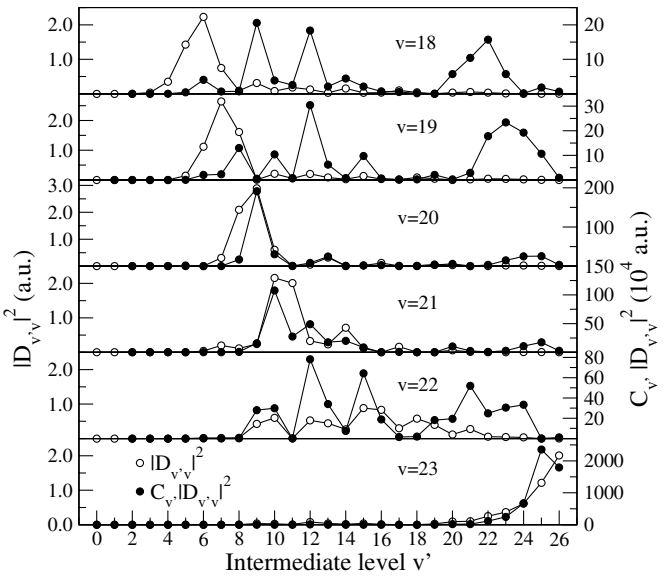

Fig. 6. Same as Figure 3 for $v = 18$ to 23 of the X state.

Table 3. One-photon $K^{(1)}$ and two-photon $K^{(2)}$ rate coefficients, and the total formation rate R for a given target state v of $X^1\Sigma^+$ state of ^{7}LiH via the intermediate level v' of $A^1\Sigma^+$ with the largest value for $C_{v'}|D_{v'v}|^2$. Powers of ten are given in square brackets.

v	v'	$C_{v'}\lvert D_{v'v}\rvert^2$ (a.u.)	$\mathsf{K}^{(1)}_{v'}$ (cm^3/s)	$\mathsf{K}^{(2)}_{vv'}$ (cm^3/s)	R_v (cm^{-3} s^{-1})
0	9	6.4 [4]	6.0 [−12]	2.8 [−11]	2.798 [11]
1	12	9.1 [4]	1.3 [−11]	4.0 [−11]	4.024 [11]
2	24	9.2 [4]	1.0 [−10]	4.0 [−11]	4.048 [11]
3	25	2.1 [5]	1.7 [−10]	9.0 [−11]	9.008 [11]
4	25	1.2 [5]	1.7 [−10]	5.5 [−11]	5.456 [11]
5	12	9.2 [4]	1.3 [−11]	4.1 [−11]	4.057 [11]
6	24	1.7 [5]	1.0 [−10]	7.7 [−11]	7.660 [11]
7	12	9.1 [4]	1.3 [−11]	4.0 [−11]	4.012 [11]
8	22	1.2 [5]	4.3 [−11]	5.4 [−11]	5.371 [11]
9	25	2.1 [5]	1.7 [−10]	9.1 [−11]	9.103 [11]
10	12	8.9 [4]	1.3 [−11]	3.9 [−11]	3.869 [11]
11	24	2.3 [5]	1.0 [−10]	1.0 [−10]	9.981 [11]
12	12	1.5 [5]	1.3 [−11]	6.5 [−11]	6.521 [11]
13	22	1.8 [5]	4.3 [−11]	8.0 [−11]	7.960 [11]
14	25	2.9 [5]	1.7 [−10]	1.2 [−10]	1.274 [11]
15	22	1.2 [5]	4.3 [−11]	5.2 [−11]	5.233 [11]
16	24	2.5 [5]	1.0 [−10]	1.1 [−10]	1.115 [12]
17	25	2.9 [5]	1.7 [−10]	1.2 [−10]	1.266 [12]
18	9	2.1 [5]	6.0 [−12]	9.0 [−11]	9.039 [11]
19	12	3.0 [5]	1.3 [−11]	1.3 [−10]	1.339 [12]
20	9	1.9 [6]	6.0 [−12]	8.4 [−10]	8.415 [12]
21	10	1.0 [6]	4.7 [−12]	4.7 [−10]	4.738 [12]
22	12	7.8 [5]	1.3 [−11]	3.4 [−10]	3.435 [12]
23	25	2.4 [7]	1.7 [−10]	1.0 [−08]	1.036 [14]

value occurs is also listed in Table 3. For each target level v, there are often several intermediate levels v' that give a large product $C'_v|D_{v'v}|^2$, and those levels could also be used, although with less efficiency. For example, for $v = 0$, the largest product arises from $v' = 9$, but $v' = 12$ is just slightly smaller. For $v = 1$, $v' = 12$ clearly gives the largest value, followed by $v' = 15$, and then $v' = 10, 20-25$: these

last levels have similar values (roughly 20% of $v' = 12$). Although in Table 3 we give the numbers for v' with the largest value, other intermediate levels might be more advantageous for certain experimental setups (e.g., laser frequencies available in a given experiment). As seen from Table 3, the maximum value of $C'_v|D_{v'v}|^2$ varies roughly between 10^5 a.u. and 10^7 a.u.

If we express the photoassociation rates $\mathsf{K}^{(1)}$ and $\mathsf{K}^{(2)}$ in terms of the various experimental parameters, we find for ^{7}Li and H

$$\mathsf{K}^{(1)}_{v'}(T, I_1) = 9.0 \times 10^{-24} I_1 \frac{C_{v'}}{T} \text{ cm}^3/\text{s} , \qquad (10)$$

and

$$\mathsf{K}^{(2)}_{vv'}(T, \{L\}) = 1.1 \times 10^{-19} I_1 I_2 \frac{C_{v'}}{T} \frac{|D_{vv'}|^2}{\Delta^2} \text{ cm}^3/\text{s} . \quad (11)$$

In these expressions, T is in Kelvin, I_1 and I_2 in W/cm^2, $C_{v'}$ and $|D_{vv'}|^2$ in a.u., and Δ in MHz. For the maximum values of $C_{v'}|D_{vv'}|^2$ in Table 3, we give the rates for typical experimental parameters; we assume $I_1 = I_2 =$ 1000 W/cm^2, $T = 1$ mK, and $\Delta = 500$ MHz (so that $\Delta \gg \gamma_{v'}$ for all v'). The rate coefficient $\mathsf{K}^{(1)}$ for the best intermediate level combinations range from 4.7×10^{-12} to 1.7×10^{-10} cm^3/s, while $\mathsf{K}^{(2)}$ varies between 2.8×10^{-11} and 8.4×10^{-10} cm^3/s, except for the last level, $v = 23$, where $\mathsf{K}^{(2)} = 1.0 \times 10^{-8}$ cm^3/s.

A rate of molecules formed per second per unit volume is obtained if we multiply the photoassociation rate by the square of the gas density n of the least abundant component, i.e. $\mathsf{R} = n^2\mathsf{K}^{(2)}$. These numbers are given in the final column of Table 3, assuming that $n \sim 10^{11}$ cm^{-3}. Typical values for R are of the order of 1×10^{12} molecules/cm^3/s, with a maximum for $v = 20$ of 8.5×10^{12}. We regard the huge molecule formation rate for $v = 23$ as extremely uncertain, due to the proximity of this level to the dissociation limit. If the typical size of the volume which can be interrogated by the lasers is of the order of 10^{-6} cm^3, then overall molecule formation rates could be approximately 1×10^6 molecules/s.

Each target level v in the ground state, except for $v = 0$, will radiatively cascade to lower-lying vibrational levels of the $X^1\Sigma^+$ state within τ_v, as given in Table 2. Because of the large dipole moment in the X state, the lifetimes are relatively short (∼4 ms), and therefore most molecules will relax to $v = 0$, even though higher levels may originally be populated in this stimulated Raman process. Because of the $\Delta J = \pm 1$ selection rule, a distribution of rotational levels, for $v = 0$, will result from the cascade. The lifetime for decay of the $v = 0$ rotational levels will be much longer than that for the excited vibrational levels. The lifetime depends very strongly on J. For instance, for $v = 0, J = 1$ the lifetime is 83 s, whereas for $v = 0, J = 10$ the lifetime is 62 ms [28].

In the cascade process, the molecules will emit infrared photons. It is interesting to calculate the recoil momentum experienced by the LiH molecule associated with the emission of a photon, in order to see if the energy gained might be enough to remove the molecule from the trap. For a photon of 1330 cm^{-1}, which is the transition energy for $v = 1$ to $v = 0$ in the $X^1\Sigma^+$ state, the recoil energy imparted to the LiH is ∼20 nK. Given a generic trap depth of a few mK, it is clear that the recoil energy should not cause significant trap loss. Even if cascade occurs from level $v = 15$, for instance, the photons in each transition will be emitted in random directions, and the net recoil momentum should be statistically no larger than that from the last transition to $v = 0$. For $v > 11$, $\Delta v = 2$ or $\Delta v = 3$ transitions may dominate the cascade. Even then the recoil energy will be less than 1 μ K. For $v < 10$, however, $\Delta v = 1$ transitions are most probable. A detailed calculation taking account of the rotational population in the cascade is underway.

6 Conclusions

We have explored the possibility of producing polar molecules, namely lithium hydride, in the electronic ground state via a two-photon Raman transition scheme. We have concentrated our efforts on the singlet transition through the intermediate excited electronic state $A^1\Sigma^+$, and found that sizable steady state rates can be achieved for almost all target states $(v, J = 0)$ of the $X^1\Sigma^+$ state, using standard experimental parameters and choosing the appropriate intermediate level v'. Significant populations of $v = 0$ molecules can be obtained as the vibrational levels populated by the stimulated Raman process decay through cascade emission in the infrared. The recoil momentum does not appear to be large enough to cause significant trap loss. Current work by the authors indicates that the $B^1\Pi$ state of LiH may be a more favorable intermediate state to consider, as its bound vibrational levels overlap more favorably with continuum levels of the X state.

The authors would like to thank A. Dalgarno and D. Kleppner for fruitful discussions. The work of E.T.-J. and R.C. was supported in part by the University of Connecticut Research Foundation, and the work of K.K. by the National Science Foundation through a grant for the Institute for Theoretical Atomic Molecular and Optical Physics at Harvard University and Smithsonian Astrophysical Observatory.

References

1. S. Jochim, M. Bartenstein, A. Altmeyer, G. Hendl, S. Riedl, C. Chin, J.H. Denschlag, R. Grimm, Science **302**, 2101 (2003); Science Express, 13 November 2003
2. M. Greiner, C.A. Regal, D.S. Jin, Nature **426**, 537 (2003)
3. M.W. Zwierlein, C.A. Stan, C.H. Schunck, S.M.F. Raupach, S. Gupta, Z. Hadzibabic, W. Ketterle, Phys. Rev. Lett. **91**, 250401 (2003)
4. K. Xu, T. Mukaiyama, J.R. Abo-Shaeer, J.K. Chin, D. Miller, W. Ketterle, Phys. Rev. Lett. **91**, 210402 (2003)
5. L. Santos, G.V. Shlyapnikov, P. Zoller, M. Lewenstein, Phys. Rev. Lett. **85**, 1791 (2000)

6. G. Modugno et al., Science **294**, 1320 (2001); M. Inguscio, Les Houches, March 2002
7. M. Modugno, F. Ferlaino, F. Riboli, G. Roati, G. Modugno, M. Inguscio, prepint `arXiv:cond-mat/0306279`
8. A. Simoni, F. Ferlaino, G. Roati, G. Modugno, M. Inguscio, Phys. Rev. Lett. **90**, 163202 (2003)
9. B. Damski, L. Santos, E. Tiemann, M. Lewenstein, S. Kotochigova, P. Julienne, P. Zoller, Phys. Rev. Lett. **90**, 110401 (2003)
10. A.J. Kerman, J.M. Sage, S. Sainis, T. Bergeman, D. DeMille, Phys. Rev. Lett. **92**, 033004 (2004)
11. A.J. Kerman, J.M. Sage, S. Sainis, T. Bergeman, D. DeMille, Phys. Rev. Lett. **92**, 153001 (2004)
12. M.E. Holmes, M. Tscherneck, P.A. Quinto-Su, N.P. Bigelow, Phys. Rev. A **69**, 063408 (2004)
13. M. Mudrich, S. Kraft, K. Singer, R. Grimm, A. Mosk, M. Weidemüller, Phys. Rev. Lett. **88**, 253001 (2002)
14. K. Kirby, R. Côté, E. Taylor-Juarros, unpublished
15. D. Kleppner, private communication
16. P. Pillet et al., J. Phys. B **30**, 2801 (1997)
17. J.L. Bohn, P.S. Julienne, Phys. Rev. A **54**, R4637 (1996)
18. R. Côté, A. Dalgarno, Phys. Rev. A **58**, 498 (1998)
19. E.P. Wigner, Phys. Rev. **73**, 1002 (1948)
20. R. Côté, M.J. Jamieson, Z.-C. Yan, N. Guem, G.-H. Jeung, A. Dalgarno, Phys. Rev. Lett. **84**, 2806 (2000)
21. N. Geum et al., J. Chem. Phys. **115**, 5984 (2001)
22. H. Partridge, S. Langhoff, W.T. Zemke, W.C. Stwalley, J. Chem. Phys. **75**, 2299 (1981)
23. W.T. Zemke, private communication
24. K.K. Docken, J. Hinze, J. Chem. Phys. **57**, 4928 (1972)
25. H. Partridge, S. Langhoff, J. Chem. Phys. **74**, 2361 (1981)
26. W.I. McAlexander, E.R.I. Abraham, R.G. Hulet, Phys. Rev. A **54**, R5 (1996)
27. W.T. Zemke, J.B. Crooks, W.C. Stwalley, J. Chem. Phys. **68**, 4628 (1978)
28. W.T. Zemke, W.C. Stwalley, J. Chem. Phys. **73**, 5584 (1980)